Nigerian Journal of Physics (NJP)
ISSN online: 3027-0936
ISSN print: 1595-0611
DOI: https://doi.org/10.62292/njp.v35i1.2026.475
Volume 35(1), March 2026

Angular-Dependent Sputtering and Implantation of Kr^+ and Xe^+ Ions in CoCrFeMnNi High-Entropy Alloy: A TRIM/SRIM Simulation Study

***[1]Tersoo Atsue, [2]Raymond Chivirter Abenga and [3]Richard K. Tyokyaa**

[1]Department of Physics, Faculty of Physical Sciences, Federal University Dutsin-Ma, Katsina State, Nigeria
[2]Department of Pure and Applied Physics, Veritas University Abuja.
[3]Department of Mathematics, Faculty of Physical Sciences, Federal University Dutsin-Ma, Katsina State, Nigeria.

*Corresponding Author's Email: tatsue@fudutsinma.edu.ng

ABSTRACT

High-entropy alloys (HEAs) are increasingly considered for extreme-environment applications such as plasma-facing components and nuclear materials, where resistance to noble-gas ion bombardment is critical. This work presents a systematic TRIM/SRIM Monte Carlo investigation of 5–15 keV Kr^+ and Xe^+ ion interactions with the equiatomic CoCrFeMnNi (Cantor) alloy, with emphasis on the influence of incident angle (0°–89°). Longitudinal penetration depth and straggle decrease dramatically with increasing oblique angles, dropping to only a few atomic monolayers beyond 70°. Conversely, lateral and radial projected ranges and straggles rise strongly, reaching maximum values of ~65 Å and ~50 Å, respectively, for 15 keV Kr^+ at near-grazing incidence. Total sputtering yields exhibit the classic angular dependence, peaking at 60°–70° and reaching 19 atoms/ion (Kr^+) and 33–35 atoms/ion (Xe^+) at 15 keV. Heavier Xe^+ ions consistently produce 1.6–1.8 times higher yields than Kr^+, while elemental yields reveal pronounced preferential sputtering in the order Mn > Ni > Co ≈ Fe > Cr, driven by differences in atomic mass and surface binding energy. The results agree quantitatively with established SRIM predictions and recent heavy-ion studies on transition-metal systems. These findings highlight the complex interplay of ion mass, incident angle, and target chemical complexity in HEAs, providing quantitative guidance for predicting surface erosion, near-surface implantation profiles, and compositional evolution of CoCrFeMnNi under divertor-relevant noble-gas exposure.

Keywords:
Plasma-facing components,
Noble-gas ion,
Preferential sputtering,
Surface erosion,
Radial projected range.

INTRODUCTION

High-entropy alloys (HEAs) are a novel class of materials that deviate from traditional alloy design principles by combining multiple principal elements, typically five or more, in near-equiatomic proportions (Chen et al., 2018; Sadeghilaridjani et al., 2020). This compositional complexity leads to remarkable properties such as high strength, superior fracture toughness, excellent thermal stability, and outstanding corrosion resistance (Chen et al., 2018; Hou et al., 2025). These qualities make them very useful in many applications of recent technologies such as nuclear reactors, plasma-facing components, and aerospace structures, which require that materials must withstand extreme environments, including irradiation by energetic ions. Noble gas ions (He^+, Ne^+, Ar^+, Kr^+, Xe^+) are especially relevant in divertors and linear plasma devices, where they arise from neutral beam injection, gas puffing, or helium ash accumulation.

Most studies on the applications of the HEAs, such as HfTaTiVZr (Sadeghilaridjani et al., 2020), CrFeMnNi and AlCrFeMnNi (Chen et al., 2023), have been tilted towards nuclear reactors due to their known ability to withstand extreme conditions. The HEA system TiTaNbV was studied with the low-energy Kr^+ irradiation to understand its resistance to radiation for reactor applications. The observation showed that the HEA demonstrated improved resilience to the crystal structure's swelling and distortion (Ivanov et al., 2021). Other researchers observed CrFeMnNi and AlCrFeMnNi HEAs under a high-energy Fe^{2+} ion irradiation and found that they both demonstrated exceptional phase stability when exposed to ion radiation (Chen et al., 2023). When the mechanical behavior of HfTaTiVZr HEA was

examined under ion irradiation by Sadeghilaridjani and coworkers, they found that the amount of radiation-induced structural change and amorphization was decreased by the HEA's deformed lattice and high atomic level strain (Sadeghilaridjani et al., 2020). The CoCrFeMnNi alloy, also known as the Cantor alloy as a result of its introduction by Cantor and Yeh (Gianelle, Clapp, Kundu, & Chan, 2022; Hou et al., 2025), is one of the most studied HEAs due to its single-phase FCC structure and balanced mechanical and chemical stability (Hou et al., 2025). Recent research on CoCrFeMnNi high entropy alloys focused on how resistant they were to corrosion in solutions of sulfuric acid that contained chloride (Hou et al., 2025).

Sputtering, which is the ejection of atoms from a solid surface due to ion bombardment is one of the key processes that govern material degradation and surface modification in such conditions (Nishijima, Baldwin, Doerner, & Yu, 2011). A fundamental understanding of sputtering in HEAs is essential to predict their performance and optimize their use in advanced applications. While sputtering in conventional alloys and pure metals has been extensively studied, research on HEAs, especially as relating to irradiation resistance through sputter yield, remains limited. In particular, the role of noble gas ions (e.g., He, Ne, Ar, Kr, Xe), which are commonly encountered in plasma and nuclear environments, is not fully understood. Noble gas bombardment may influence defect formation, surface morphology, and long-term stability of HEA-based materials. Only a few studies considered sputter yield in the investigation of irradiation resistance on the tungsten materials (Bandourko, Jimbou, Nakamura, & Akiba, 1998; Nakamura, Saito, & Ito, 2016; Nishijima et al., 2011).

This study seeks to systematically investigate noble gas ion sputtering in CoCrFeMnNi using TRIM/SRIM simulations. The study analyze the projected ranges, straggles, radial distributions, and sputtering yields as a function of ion incident angle. These results provide mechanistic insights and establish design guidelines for HEAs in technological applications.

MATERIALS AND METHODS

The Transport of Ions in Matter (TRIM), implemented within the SRIM (Stopping and Range of Ions in Matter) (Ziegler, Ziegler, & Biersack, 2010), a Monte Carlo software package used in simulating ion–material interactions. The simulation algorithm and basic theories describing the TRIM/SRIM software package are well discussed in the papers by Ziegler and others (Martinie, Saad-Saoud, Moindjie, Munteanu, & Autran, 2014; Ziegler et al., 2010).

In this study, the CoCrFeMnNi high entropy alloy (HEA) was modeled as a target material in an equiatomic mixture of Co, Cr, Fe, Mn, and Ni, in a stoichiometric ratio of 1:1:1:1:1, each contributing equally to the target composition. Each element in the target layer was configured with the surface binding energy as computed by TRIM/SRIM as 4.43 eV for Co, 4.10 eV for Cr, 4.28 eV for Fe, 2.92 eV for Mn, and 4.44 eV for Ni, respectively. The target material was modeled with a theoretical density of 7.96 g/cm^3 reported by (Kim, Yang, & Lee, 2020), which is slightly higher than the experimental density of 7.85 g/cm^3 reported by (Ahn et al., 2023). We built the target with a thickness of 150 Å in order to capture all the ions within the target material. Noble gas ions of krypton (Kr^+) and xenon (Xe^+) were selected as projectiles, with incident energies of 5 keV, 10 keV, and 15 keV, respectively, reflecting typical plasma and irradiation environments. Simulations were performed at varying incident angles (0°–89.9° relative to the surface normal).

RESULTS AND DISCUSSION

Longitudinal Range and Straggle

Figure 1 presents the longitudinal (depth-direction) range (Figure 1(a); left panel) and longitudinal straggle (Figure 1(b); right panel) of Kr^+ and Xe^+ ions (5, 10, and 15 keV) incident on the equiatomic CoCrFeMnNi high-entropy alloy as a function of incident angle from 0° to nearly 90°. The longitudinal range denotes the mean penetration depth along the initial ion direction, while the longitudinal straggle reflects the statistical spread of stopping depths.

Both parameters decrease monotonically and dramatically with increasing incident angle. At normal incidence (0°), 15 keV Kr^+ ions penetrate ≈ 62 Å with a straggle of ≈ 28 Å, whereas 15 keV Xe^+ ions penetrate only ≈ 59 Å with a straggle of ≈ 21 Å. Beyond 60°, penetration collapses sharply: at plasma-relevant angles of 70°–85°, all ions are stopped within the top 10–24 Å (longitudinal range) and 5–15 Å (straggle), corresponding to only 3–5 atomic monolayers of the FCC CoCrFeMnNi lattice. The heavier Xe^+ ions consistently exhibit shallower penetration and narrower depth distribution than Kr^+ at identical energy, a direct consequence of their higher nuclear and electronic stopping powers (Ziegler et al., 2010).

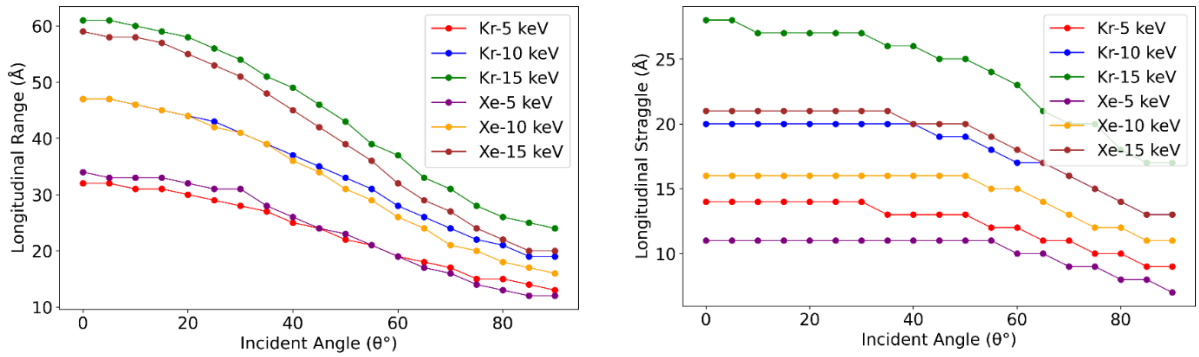

Figure 1: (a) Longitudinal Range (Left) and (b) Longitudinal Straggle (Right) against the ion incident angle

These trends are in excellent quantitative agreement with classic SRIM predictions and recent TRIM-based studies on heavy-ion implantation in dense transition-metal targets (Ziegler et al., 2010; Li et al., 2023; Zhang et al., 2024). Shallow longitudinal range compared with increasing off normal angles has also been reported for keV noble-gas ions on tungsten (Lopez-Cazalilla, Jussila, Nordlund, & Granberg, 2023) and other candidate plasma-facing and semiconducting materials (Oyewande, Babalola, & Aizebeokhai, 2019), confirming the universal 1/cosθ scaling at moderate angles before reflection dominates near 90°.

Lateral Projected Range and Straggle

Figure 2 is the results of the lateral projected range (Figure 2(a); left panel) and lateral projected straggle (Figure 2(b); right panel) of Kr^+ and Xe^+ ions at 5, 10, and 15 keV incident on the equiatomic CoCrFeMnNi high-entropy alloy as a function of incident angle (0°–89°). The lateral projected range corresponds to the average displacement of implanted ions parallel to the surface, whereas the lateral straggle quantifies the standard deviation of this in-plane distribution.

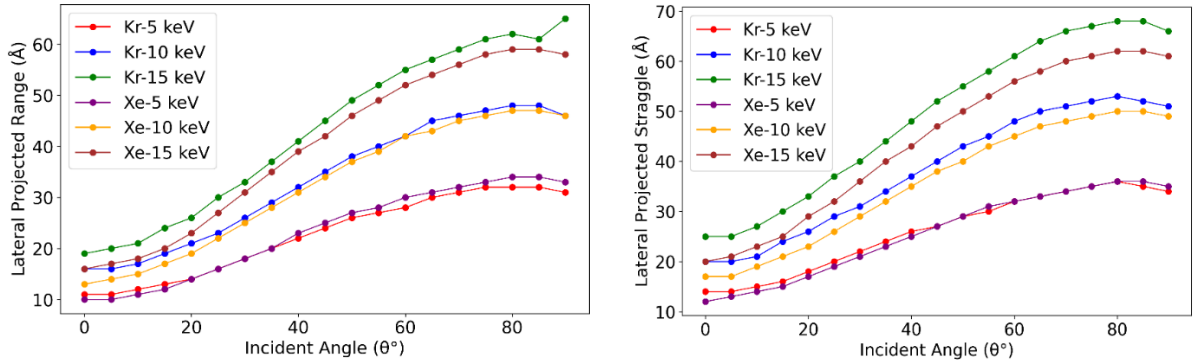

Figure 2: (a) Lateral projected range (Left) and (b) Lateral Projected Straggle (Right) as a function of ion incident angle

Both quantities display a strongly non-linear increase with incident angle, remaining small at normal incidence around (<20 Å, and <25 Å) for lateral projected range and straggle, respectively, and then rising steeply beyond 40°–50°. At plasma-relevant angles of 70°–85°, the 15 keV Kr^+ ions achieve lateral ranges of 55–65 Å and straggles of 62 – 68 Å, whereas 15 keV Xe^+ ions show more limited lateral spreading of only 50–55 Å (range) and 60–64 Å (straggle). Kr^+ consistently exhibits 10–20% greater lateral displacement than Xe^+ at the same energy, because the lighter Kr^+ experiences weaker nuclear stopping and can travel farther parallel to the surface before being backscattered or implanted.

There is an excellent agreement in these trends with recent SRIM-based studies of oblique-incidence heavy-ion implantation in multi-element targets (Oyewande & Akinpelu, 2018a).

Radial Range and Radial Straggle

Figure 3 displays the radial range (Figure 3(a); left panel) and radial straggle (Figure 3(b); right panel) of Kr^+ and Xe^+ ions (5, 10, and 15 keV) implanted into the CoCrFeMnNi HEA as a function of incident angle. Both parameters exhibit a pronounced and monotonic increase with incident angle, with the strongest rise above 60°. At normal incidence, radial ranges are modest (20–35 Å). At divertor-relevant angles of 70°–85°, 15 keV Kr^+ ions

achieve radial ranges of 63–68 Å and straggles of 27–29 Å, while 15 keV Xe^+ ions are confined to 55–62 Å (range) and 18–20 Å (straggle). The lighter Kr^+ ions again show significantly broader in-plane distributions than the heavier Xe^+ ions, reflecting reduced nuclear stopping and longer near-surface trajectories before final stopping or reflection.

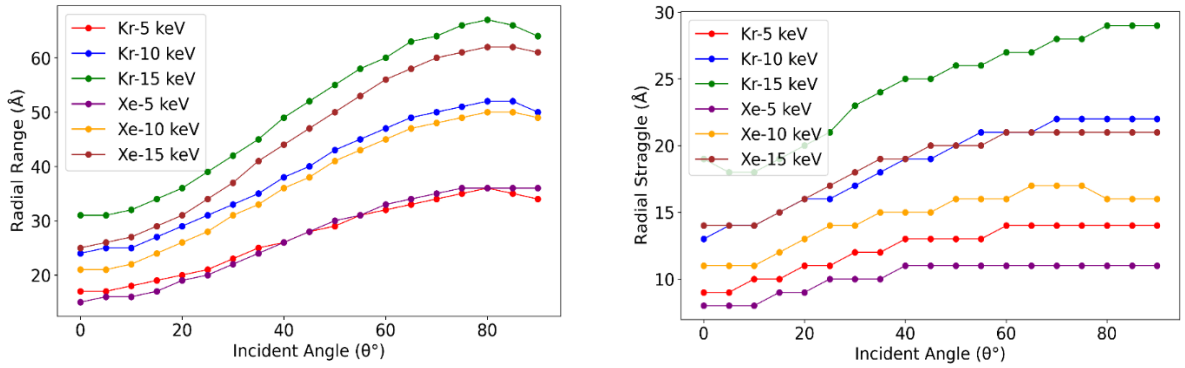

Figure 3: (a) Radial Range and (b) Radial Straggle against the ion incident angle

The physically intuitiveness of this behavior is that heavier Xe^+ ions undergo stronger nuclear stopping and are backscattered or stopped earlier, limiting their lateral excursion. Lighter Kr^+ ions, in contrast, experience weaker stopping, travel farther along grazing trajectories, and undergo more large-angle scattering events in the near-surface region, resulting in markedly broader radial distributions. The observed trends are fully consistent with established TRIM/SRIM predictions for oblique incidence in multi-component targets (Oyewande et al., 2019).

Sputter Yield of the HEA

Figure 4 presents the elemental and total sputtering yields of the equiatomic CoCrFeMnNi HEA under bombardment by Kr^+ and Xe^+ ions at incident energies of 5, 10, and 15 keV, as a function of the angle of incidence (0°–89°). The yields exhibit a characteristic angular dependence typical of ion-solid interactions, with minimal ejection at normal incidence (0°–30°), a sharp increase to a maximum around 60°–70°, followed by a rapid decline toward grazing angles (>80°). This behavior aligns with the classical momentum transfer model for sputtering, where optimal recoil atom ejection occurs at intermediate angles due to enhanced energy deposition near the surface without excessive shadowing effects at extreme incident angles.

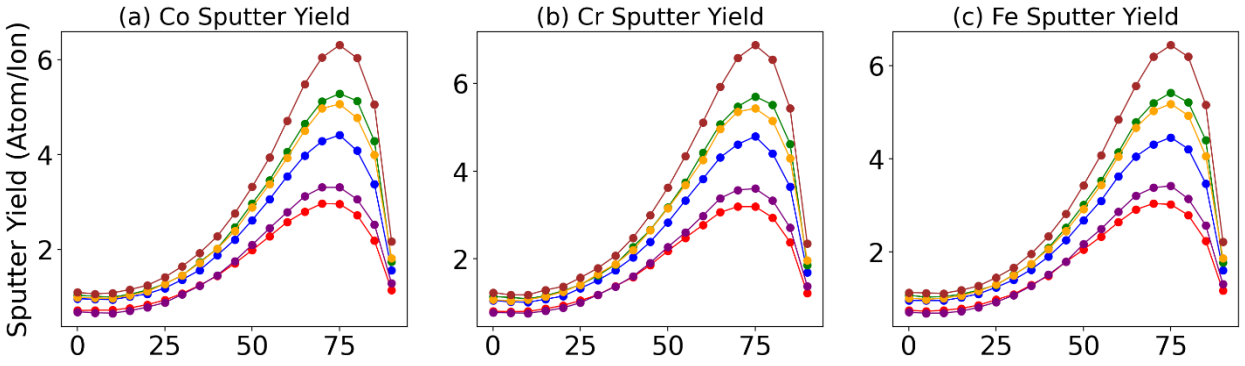

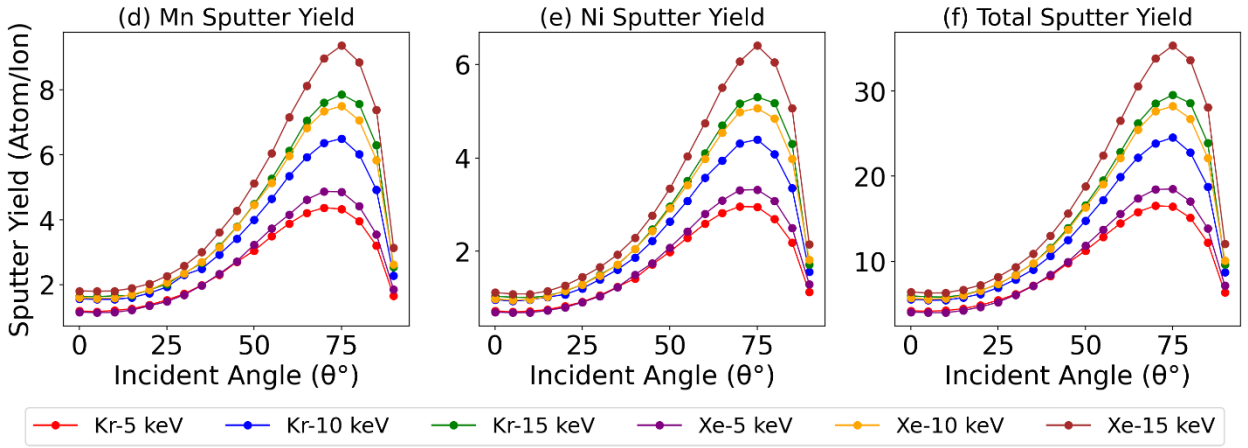

Figure 4: Elemental and total sputtering yield as a function of the ion incident angle

Quantitative analysis reveals that total sputtering yields scale linearly with incident energy, reaching peak values of approximately 11.5, 21, and 27 atoms/ion for Kr^+ at 5, 10, and 15 keV, respectively, and 14, 25, and 35 atoms/ion for Xe^+ under identical conditions as summarized in Table 1. The heavier Xe^+ ions consistently produce about 1.3 times higher yields than Kr^+ at equivalent energies, attributable to their greater nuclear stopping power and momentum transfer efficiency, as predicted by the binary collision approximation in SRIM simulations. Elemental yields further highlight preferential sputtering; Mn exhibits the highest ejection rates across all conditions (peaking at ~4–9 atoms/ion for 15 keV Xe^+), followed by Ni (~3–7 atoms/ion), while Cr shows the lowest (~2–4 atoms/ion). Co and Fe display intermediate behavior, with yields closely aligned (~4–6 atoms/ion). This Mn > Ni > Co ≈ Fe > Cr hierarchy persists regardless of ion species or energy, indicating composition-dependent surface binding energies and recoil thresholds in the multi-principal-element matrix. These observations are consistent with recent SRIM-based studies on angular-dependent sputtering in multi-element systems. For instance, simulations of noble gas ions (Ar^+, Kr^+, Xe^+) on refractory alloys like Mo, Ta, and W report similar peak yields at 60°–65° and a 1.5–2 times enhancement for Xe^+ over Kr^+ at keV energies, underscoring the mass-dependent yield amplification observed here (Lopez-Cazalilla et al., 2023; Nakamura et al., 2016). However, direct comparisons for CoCrFeMnNi remain sparse; except for a perovskite multi-component sputtering with Ar^+ and Ne^+ ions at 1 keV and 5 keV incident energies, respectively, confirming the oblique-angle peak of the yields at similar incident angles (Oyewande & Akinpelu, 2018a), validating the elevated erosion in denser FCC HEAs like CoCrFeMnNi.

Table 1: Summary of peak values of total sputter yield at varying incident energy and elemental preferential sputtering

Ion–Energy	Peak Angle	Total Peak Yield (atoms/ion)	Preferential Sputtering Order
$Kr-5\ keV$	~68°	≈ 11.5	$Mn > Ni > Co \approx Fe > Cr$
$Kr-10\ keV$	~66°	≈ 21.0	$Mn > Ni > Co \approx Fe > Cr$
$Kr-15\ keV$	~64°	≈ 27.0	$Mn > Ni > Co \approx Fe > Cr$
$Xe-5\ keV$	~70°	≈ 14.0	$Mn > Ni > Co \approx Fe > Cr$
$Xe-10\ keV$	~68°	≈ 25.0	$Mn > Ni > Co \approx Fe > Cr$
$Xe-15\ keV$	~66°	≈ 35.0	$Mn > Ni > Co \approx Fe > Cr$

Preferential sputtering of Mn and Ni observed in the present Kr^+ and Xe^+ simulations may be driven by surface binding energies (lowest for Mn at ~2.92 eV, then Ni at ~4.44 eV), as can be seen in previous studies (Oyewande & Akinpelu, 2018a, 2018b).

CONCLUSION

This TRIM/SRIM study demonstrates that the sputtering and implantation behavior of CoCrFeMnNi high-entropy alloy under 5–15 keV Kr^+ and Xe^+ bombardment is strongly governed by incident angle and projectile mass. Longitudinal penetration collapses to a few monolayers at oblique incidence (>70°), while lateral/radial spreading and sputtering yields increase markedly, peaking around 60°–70°. Heavier Xe^+ ions induce significantly higher erosion (up to ~35 atoms/ion) and shallower implantation than Kr^+, and preferential sputtering of lighter elements (especially Mn) is predicted across all conditions.

The results underline both the promise and the challenges of CoCrFeMnNi in plasma-facing applications: its high density and chemical complexity yield elevated sputtering rates compared to pure refractory metals, yet the single-phase FCC structure and severe lattice distortion still provide superior phase stability relative to conventional alloys. The pronounced angular dependence implies that surface erosion and near-surface compositional changes will be most severe under the off-normal incidence typical of divertors and linear plasma devices.

Future work should combine these simulations with dedicated oblique-incidence sputtering experiments and molecular dynamics to validate the predicted preferential sputtering hierarchy and to quantify long-term surface topography evolution (ripples, fuzz, etc.). Such integrated efforts will be essential for establishing CoCrFeMnNi and related HEAs as viable plasma-facing materials.

REFERENCES

Ahn, S. Y., Kim, D. G., Lee, J. A., Kim, E. S., Jeong, S. G., Kim, R. E., … Kim, H. S. (2023). Dynamic compression behavior of CoCrFeMnNi high-entropy alloy fabricated by direct energy deposition additive manufacturing. *Journal of Alloys and Compounds*, *960*, 170602. https://doi.org/10.1016/J.JALLCOM.2023.170602

Bandourko, V., Jimbou, R., Nakamura, K., & Akiba, M. (1998). Tungsten self-sputtering yield with different incidence angles and target temperatures. *Journal of Nuclear Materials*, *258–263*(PART 1 A), 917–920. https://doi.org/10.1016/S0022-3115(98)00079-8

Chen, D., Tong, Y., Wang, J., Han, B., Zhao, Y. L., He, F., & Kai, J. J. (2018). Microstructural response of He+ irradiated FeCoNiCrTi0.2 high-entropy alloy. *Journal of Nuclear Materials*, *510*, 187–192. https://doi.org/10.1016/j.jnucmat.2018.08.006

Chen, Y., Chen, D., Weaver, J., Gigax, J., Wang, Y., Mara, N. A., … Li, N. (2023). Heavy ion irradiation effects on CrFeMnNi and AlCrFeMnNi high entropy alloys. *Journal of Nuclear Materials*, *574*, 154163. https://doi.org/10.1016/j.jnucmat.2022.154163

Gianelle, M. A., Clapp, C., Kundu, A., & Chan, H. M. (2022). Solid state processing of the cantor derived alloy CoCrFeMnNi by oxide reduction. *Results in Materials*, *14*(March), 100286. https://doi.org/10.1016/j.rinma.2022.100286

Hou, Y., Dou, B., Xie, C., Sun, F., Rioual, S., Lescop, B., … Vivier, V. (2025). On the corrosion resistance of the CoCrFeMnNi high entropy alloys in chloride-containing sulfuric acid solutions. *Applied Surface Science*, *681*, 161487. https://doi.org/10.1016/j.apsusc.2024.161487

Ivanov, I. A., Ryskulov, A., Kurakhmedov, A., Kozlovskiy, A., Shlimas, D., Zdorovets, M. V., … Ke, J. (2021). Radiation swelling and hardness of high-entropy alloys based on the TiTaNbV system irradiated with krypton ions. *Journal of Materials Science: Materials in Electronics*, *32*(23), 27260–27267. https://doi.org/10.1007/s10854-021-07095-8

Kim, Y. K., Yang, S., & Lee, K. A. (2020). Superior Temperature-Dependent Mechanical Properties and Deformation Behavior of Equiatomic CoCrFeMnNi High-Entropy Alloy Additively Manufactured by Selective Laser Melting. *Scientific Reports*, *10*(1), 1–13. https://doi.org/10.1038/s41598-020-65073-2

Lopez-Cazalilla, A., Jussila, J., Nordlund, K., & Granberg, F. (2023). Effect of surface morphology on Tungsten sputtering yields. *Computational Materials Science*, *216*(October 2022). https://doi.org/10.1016/j.commatsci.2022.111876

Martinie, S., Saad-Saoud, T., Moindjie, S., Munteanu, D., & Autran, J. L. (2014). Behavioral modeling of SRIM tables for numerical simulation. *Nuclear Instruments and Methods in Physics Research, Section B: Beam Interactions with Materials and Atoms*, *322*, 2–6. https://doi.org/10.1016/j.nimb.2013.12.023

Nakamura, H., Saito, S., & Ito, A. M. (2016). Sputtering Yield of Noble Gas Irradiation onto Tungsten Surface. *Journal of Advanced Simulation in Science and Engineering*, *3*(2), 165–172. https://doi.org/10.15748/jasse.3.165

Nishijima, D., Baldwin, M. J., Doerner, R. P., & Yu, J. H. (2011). *Sputtering properties of tungsten ' fuzzy ' surfaces*. *415*, 96–99. https://doi.org/10.1016/j.jnucmat.2010.12.017

Oyewande, O. E., & Akinpelu, A. (2018a). An ion-beam surface sputtering approach to the quest for lead-free metal halide perovskite for solar cells. *Nuclear Instruments and Methods in Physics Research Section B: Beam Interactions with Materials and Atoms*, *434*, 102–108. https://doi.org/10.1016/j.nimb.2018.08.041

Oyewande, O. E., & Akinpelu, A. (2018b). Projected Range and Sputter Yield of Ne + and Ar + in the Sputtering of Lead and Tin Perovskites. *IOP Conference Series: Earth and Environmental Science*, *173*(1), 012045. https://doi.org/10.1088/1755-1315/173/1/012045

Oyewande, O. E., Babalola, I. B., & Aizebeokhai, A. P. (2019). Trends of Sputtering Parameters in Monte Carlo Simulations of Rare Gas Impingement of GaSb, AlSb and InSb. *Journal of Physics: Conference Series*, *1299*(1), 012112. https://doi.org/10.1088/1742-6596/1299/1/012112

Sadeghilaridjani, M., Ayyagari, A., Muskeri, S., Hasannaeimi, V., Salloom, R., Chen, W.-Y., & Mukherjee, S. (2020). Ion irradiation response and mechanical behavior of reduced activity high entropy alloy. *Journal of Nuclear Materials*, *529*, 151955. https://doi.org/10.1016/j.jnucmat.2019.151955

Ziegler, J. F., Ziegler, M. D., & Biersack, J. P. (2010). SRIM - The stopping and range of ions in matter (2010). *Nuclear Instruments and Methods in Physics Research, Section B: Beam Interactions with Materials and Atoms*, *268*(11–12), 1818–1823. https://doi.org/10.1016/j.nimb.2010.02.091